CHEMISTRY OF MATERIALS
Cite This: Chem. Mater. 2018, 30, 5468−5477
Article
pubs.acs.org/cm

Unraveling the Structure of Magic-Size $(CdSe)_{13}$ Cluster Pairs

Tzung-En Hsieh,[†,∥] Ta-Wei Yang,[†,∥] Cheng-Yin Hsieh,[†,∥] Shing-Jong Huang,[‡] Yi-Qi Yeh,[§] Ching-Hsiang Chen,[⊥] Elise Y. Li,*[,†] and Yi-Hsin Liu*[,†]

[†]Department of Chemistry, National Taiwan Normal University, Taipei 11677, Taiwan
[‡]Department of Chemistry, National Taiwan University, Taipei 10617, Taiwan
[§]National Synchrotron Radiation Research Center, Hsinchu 30075, Taiwan
[⊥]Graduate Institute of Applied Science and Technology, National Taiwan University of Science & Technology, Taipei 11677, Taiwan

Supporting Information

ABSTRACT: Cadmium selenide is a II−VI semiconductor model system known for its nanoparticle preparation, growth mechanism, luminescence properties, and quantum confinement studies. For the past 2 decades, various thermodynamically stable "magic-size nanoclusters (MSCs)" of CdSe have been observed, isolated, and theoretically calculated. Nevertheless, none of the proposed structures were experimentally confirmed due to the small crystal domains beyond the diffraction limit. With a combination of nondestructive SAXS, WAXS, XRD, XPS, EXAFS, and MAS NMR techniques, we were able to verify the phase transformation, shape, size dimension, local bonding, and chemical environments of $(CdSe)_{13}$ nanoclusters, which are indicative of a paired cluster model. These experimental results are consistent with the size, shape, bond lengths, dipole moment, and charge densities of the proposed "paired-tubular geometry" predicted by computational approaches. In this article, we revisit the formation pathway of the mysterious $(CdSe)_{13}$ nanoclusters and propose a paired cluster structure model for better understanding of II−VI semiconductor nanoclusters.

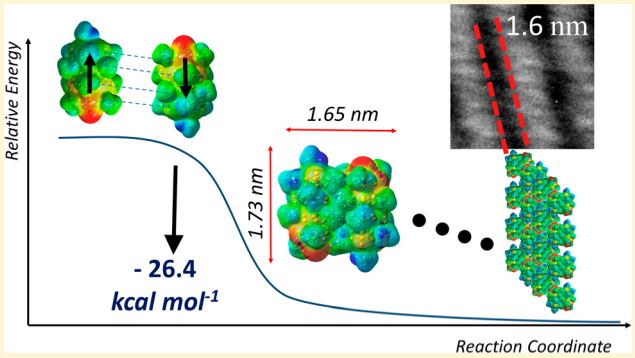

INTRODUCTION

Quantum-confined semiconductors, such as CdSe, have recently been rationally synthesized as nanosheets (2D),[3] nanowires (1D),[4] nanoparticles (0D),[5−8] and even nanoclusters (0D)[9,10] in solutions. Nanoclusters, structurally different from nanoparticles (>ca. 2 nm), with atomically defined sizes, dimensions, and geometries similar to those of molecules, have drawn the interest of researchers to study their chemical bonding and nanoparticle formation mechanism.[11] Alternatively, nanoclusters, which are smaller than nanoparticles yet are more uniform in size, can be utilized to grow ultrathin 2D materials[12,13] as well as to improve the performance of photovoltaics via self-assembly,[14,15] electroless deposition,[16] and direct patterning.[17]

$(CdSe)_{13}$ and other magic-size nanoclusters have been reported as key intermediates[1,9,18−20] and building units as a single-source precursor for the growths of CdSe 0D, 1D, and 2D quantum structures.[19−23] The structural transformation from clusters to 2D materials directly inspires the development of diluted magnetic semiconductors (DMSs) for creative magnetic applications.[24,25] For example, self-assemblies of Mn-doped $(CdSe)_{13}$[26,27] into nanoribbons significantly enhance g_{eff} values (63 → ∼600) via strong sp−d exchange couplings between localized 3d electrons and delocalized band charge carriers, revealing new insights on molecular engineering.

In recent studies, pure $(CdSe)_{13}$ clusters, which are nonemissive, have been successfully isolated and characterized by distinct absorption and mass spectroscopy.[10,14,28] Nevertheless, developments of the semiconducting nanoclusters are still limited by the difficulty in recrystallization.[29] The $(CdSe)_{13}$ core dimension has been estimated to be 0.80 nm by extrapolating the layer-to-layer d spacing in low-angle X-ray diffraction (XRD) data,[30] but a detailed crystal structure is still unknown due to poor crystallinity or short coherent lengths.[30] Unlike metal-based nanoclusters,[31] most of these semiconducting nanoclusters are neutral and have to be passivated with long alkyl chains.[10] Spontaneous self-assembly[14] of the clusters and oriented attachment[22] of the inorganic cores impede the formation of single crystals of these nanoclusters. Due to the sensitivity of the weakly passivated amine-based CdSe MSCs to ionization, mass spectroscopy (MS) is not always a supportive technique to reveal the presence and purity of CdSe MSCs while maintaining the sample stability during

Received: June 11, 2018
Revised: July 17, 2018
Published: July 17, 2018

Downloaded via SYNCHROTRON RADIATION RESEARCH on January 21, 2019 at 03:21:54 (UTC).
See https://pubs.acs.org/sharingguidelines for options on how to legitimately share published articles.

© 2018 American Chemical Society

DOI: 10.1021/acs.chemmater.8b02468
Chem. Mater. 2018, 30, 5468−5477

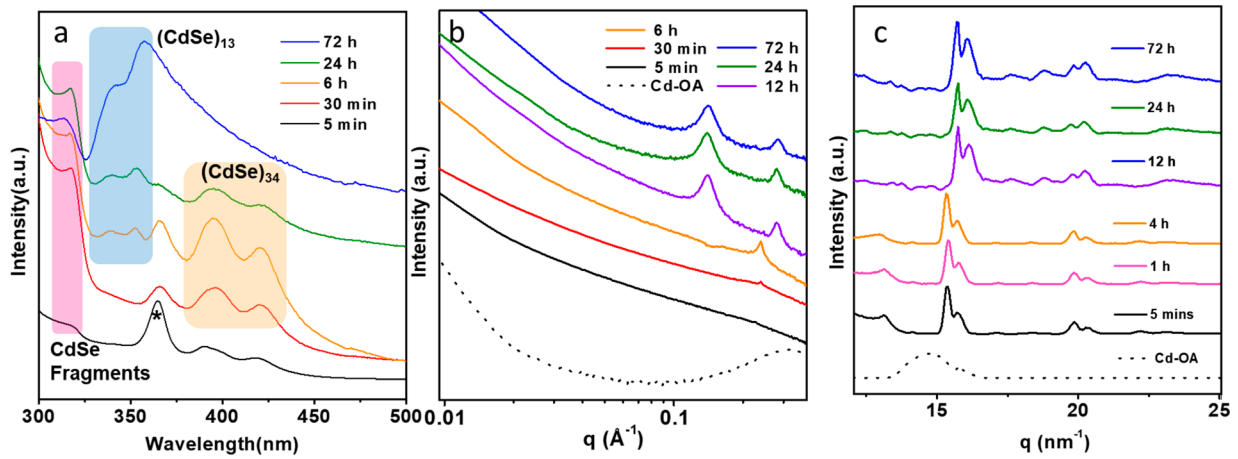

Figure 1. (a) UV−vis absorption spectra and (b) SAXS and (c) WAXS patterns of $(CdSe)_{13}$ nanoclusters formed after 5 min (black), 30 min (red), 1 h (pink, in WAXS only), 4 h (orange in SAXS/WAXS), 6 h (orange in UV), 24 h (green), and 72 h (blue). The asterisk refers to an unidentified early stage intermediate in this study, and the dotted lines in SAXS and WAXS refer to Cd−OA complexes.

the experiment.[10,21] Furthermore, direct TEM/HRTEM imaging evidence of single or few clusters[32] without sample damaging has not been acquired due to spontaneous agglomeration and particle growth under intense electron beam exposure.[10] Thus, in situ nondestructive structural analyses (e.g., pair distribution function, PDF) are suitable techniques to study local bonding information on amorphous nanoclusters or those with poor crystallinity.[29,33]

Although several geometries of $(CdSe)_{13}$ and other nanoclusters have been predicted by theoretical calculations,[34,35] none of the structures have been experimentally verified. All ultrasmall CdSe materials, including the tetrahedral $Cd_{35}Se_{20}X_{30}L_{30}$ nanoparticles,[29] single-layered 2D $CdSe(en)_{0.5}$,[36] and $(CdSe)_{13}$,[10] have been reported to show an indistinguishable absorption spectrum with an electronic transition energy of around 3.50 eV (354 nm) regardless of their stoichiometry ratios. Morphological and structural resolution of the $(CdSe)_{13}$ nanoclusters remains intriguing in terms of many fundamental aspects.

In this study, on the basis of full characterizations of nondestructive techniques to monitor growth of desired nanoclusters, we explore the true structure of $(CdSe)_{13}$ nanoclusters. Complementary small- and wide-angle X-ray scattering (SAXS, WAXS) are powerful synchrotron-based characterization tools that can reveal molecular morphology in nanometer and angstrom length scales.[33,37] Other nondestructive solid-state techniques, such as nuclear magnetic resonance (NMR) spectroscopy[38] and extended X-ray absorption fine structure (EXAFS)[39] spectroscopy, which is more informative than PDF,[29,40] allow us to probe local bonding and the chemical environment without damaging samples. We observe a novel "paring" interaction for the $(CdSe)_{13}$ MSCs that is strongly supported by our computational investigations. We believe that this comprehensive and multidisciplinary study, including chemical synthesis, physical characterizations, and theoretical calculations, shall bring valuable insights in understanding the important role of microscopic interactions in nanoclusters and the formation of 2D materials.

RESULTS AND DISCUSSION

Formation of MSCs. Sequential growths of CdSe magic-size clusters (MSCs) have been previously monitored in solution via UV−vis absorption, showing size evolution through different species to nanoparticles at 80 °C.[19,41] Here, we elucidate a $(CdSe)_{13}$ formation pathway through metastable growth of $(CdSe)_{34}$ nanoclusters at room temperature (15−25 °C) by UV−vis absorption[9] and SAXS[42] and WAXS techniques. As noted above, CdSe MSCs of various magic numbers and sizes reported with defined absorption spectra can be interconverted by varying temperatures.[21] By rational synthesis carried out in amine-based systems,[30] time-dependent growth of CdSe MSCs is able to occur at room temperature or even lower, suggesting high reactivity and lability of amine-ligated CdSe MSCs compared to carboxylate-ligated CdSe nanoparticles.[28] The absorption spectra of CdSe intermediates sampled at different periods during the synthesis (0−72 h) are compared in Figure 1a. Three predominant peaks, including one distinct absorption at 419 nm, indicate initial formation of $(CdSe)_{34}$ nanoclusters[1,21] within the first 5 min after mixing $Cd(OAc)_2$ and selenourea in octylamine. In the following 24 h, $(CdSe)_{34}$ nanoclusters coexist with other smaller nanoclusters, $(CdSe)_{13}$ (350 nm) and CdSe fragments (320 nm), as highlighted in Figure 1a. After 72 h, multiple absorption peaks converge into characteristic ones (355, 340, 314 nm) of the pure $(CdSe)_{13}$, indicative of a final thermodynamic product at room temperature. The electronic structure evidence suggests a kinetic growth pathway of metastable $(CdSe)_{34}$ conversion to $(CdSe)_{13}$ at room temperature, as previous studies have reported that $(CdSe)_{34}$ could only exist in a mixed-solvent system[43] or at low temperatures (0 °C).[21]

During the same growth period, ex situ SAXS experiments of CdSe MSCs were conducted to compare evolutions of sizes and shapes. A broad feature of a liquid-crystal-like mesophase of Cd−amine complexes[44] was initially confirmed by a broad feature in Figure 1b (0.32 $Å^{-1}$, 1.97 nm), suggesting dissolution of the cadmium salts in the long-chain solvent and the formation of amine-coordinated complexes. After injection of selenourea into Cd−amine complexes, the mesophase collapsed and reconstructed simultaneously into another lamella (2.63 nm) until a full integration into an ultimate layered structure (4.45 nm) after 24−72 h. During the growth period, the SAXS intensity continued to increase, suggesting development of the organic−inorganic hybrid aggregates and a trend of increasing electron density. The

DOI: 10.1021/acs.chemmater.8b02468
Chem. Mater. 2018, 30, 5468−5477

crystalline phases of CdSe MSCs are revealed via ex situ WAXS experiments (Figure 1c). Similar to the SAXS result, the initial mesophase shows only broad WAXS features due to limited aggregate dimension. After injection of selenourea, nucleation and growth begin, resulting in different crystal phases. Surprisingly, one phase (19.8−20.3 nm^{-1}, 3.2−3.1 Å) remains identical during the whole growth period, suggesting the persistence of the distance between certain lattice facets during the $(CdSe)_{34}$ to $(CdSe)_{13}$ transformation. Another crystal phase shows sudden shifts to wide angles (15.4 → 15.7 nm^{-1}, 4.29 → 3.99 Å) during the growth period. This sudden shifting in wide-angle *d*-spacing suggests a geometry contraction that leads to shortening of the facet distance in the final product. This phenomenon also implies an internal morphology evolution during the nanocluster formation, providing optical evidence for interconversion kinetics of $(CdSe)_{34}$ to $(CdSe)_{13}$ clusters. The growth transformation of CdSe MSCs is summarized in Scheme 1. Initially, the Cd−amine complexes

Scheme 1. Illustration of Phase Transformation from Cd Complexes, Metastable $(CdSe)_{34}$[1] (green dots) to $(CdSe)_{13}$ MSC (orange dots)[2a]

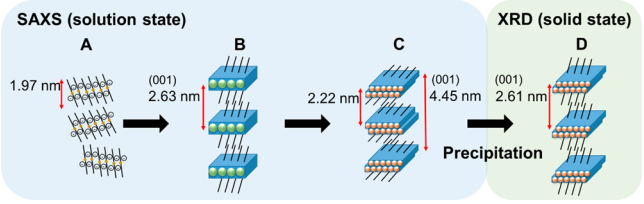

[a]The green and orange dots refer to $(CdSe)_{34}$ and $(CdSe)_{13}$ MSCs, respectively. The negative charges refer to acetate anions, and the black lines refer to the ligands.

aggregate to form 2D-like (pseudo)monolayers showing poor crystalline domains of 2.78 nm (via Scherrer equation) and a layer-to-layer *d*-spacing of 1.97 nm.[14,45] At this stage, the complexes are directly bound to octylamines, whereas the acetate anions serve as the counterions to balance the charges. Upon injection of Se precursors, the Se^{2-} complexes[46,47] replace the acetate counteranion and maintain the intrinsic layer structure by consecutive bridging Cd complexes. In the following 4 h, the intermediate $(CdSe)_{34}$ was optically observed with a layer-to-layer *d*-spacing of 2.63 nm, and it continuously converted to $(CdSe)_{13}$ with a layer-to-layer *d*-spacing of 4.45 nm. A noticeably increased layer-to-layer *d*-spacing in SAXS (4.45 nm) to almost twice that of the *d*-spacing observed in XRD (2.612 ± 0.001 nm, Figure S1) of $(CdSe)_{13}$ was completely unexpected. Sample states (from solution to solid) seem to change the layer periodicity from the monolayer $(CdSe)_{34}$ (stage B) to the bilayer $(CdSe)_{13}$ (stage C), as shown in Scheme 1. In fact, such a doubling of the (001) *d*-spacing in solution phases has been previously studied due to an offset of layer symmetry.[48] Changes of tilting and interdigitating of octylamine also occur, resulting in varied *d*-spacing between layers. In solid samples, the degrees of interdigitation and tilting are reduced due to the decreased freedom of rigid alkyl chains, and the increased layer-to-layer distance leads to an increment of (001) *d*-spacing in XRD (2.22 → 2.61 nm, from stage C to D in Scheme 1). Such a packing phenomenon of alkyl chains has been observed in oligomeric silsesquioxanes (POSS) cages[48] and ammonium ionic liquids,[49] which explains the larger *d*-spacing observed in XRD than that in SAXS. On the basis of the doubling of (001) *d*-spacing and the difference in SAXS/XRD results, a bilayer model of $(CdSe)_{13}$ is thus proposed via interconversion from the monolayer $(CdSe)_{34}$ without significantly changing the layer-to-layer distance.

To improve crystallinity, the as-made $(CdSe)_{13}$ was stored in a mixed solvent system of octylamines and trioctylphosphines. After 1 year from preparation, the color of the aged $(CdSe)_{13}$ remained white without any observable changes in the absorption spectrum (Figure S2). To our surprise, its morphology gradually transformed from a triangular (Figure 2a) into a rectangular shape (Figure 2b) in TEM images. The

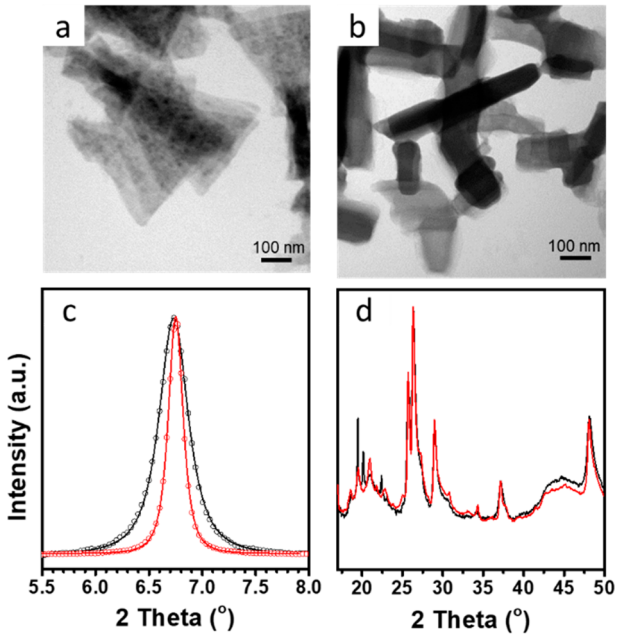

Figure 2. Representative TEM images of (a) as-made $(CdSe)_{13}$ and (b) aged $(CdSe)_{13}$ nanoclusters. (c) Low-angle (experimental and fitted) and (d) wide-angle synchrotron XRD of the above as-made (black curve) and aged (red curve) $(CdSe)_{13}$ nanoclusters.

layer-to-layer distance and the wide-angle diffraction patterns (Figure 2c,d) of the as-made and the aged products were identical, but the crystalline domains were found to slightly increase (26 → 51 nm via the Scherrer equation) after this long period of time. We also note that the aged product showed more accurate elemental analysis (EA) results for $C_8H_{19}N$ (C:H:N = 7.7:18.8:1.0) than the as-made $(CdSe)_{13}$ (C:H:N = 7.2:17.0:1.0), indicating a very time-consuming recrystallization and purification process at room temperature.

We also revisit protocols of disassembling $(CdSe)_{13}$ nanoclusters in long alky chain solvents. The as-made $[(CdSe)_{13}\ (octylamine)_{13}]$ nanoclusters originally self-assembled into sheet-like triangular lamellae (Figure 2a) in which the octylamines constitute the layer-to-layer spacer of the $(CdSe)_{13}$ lamellae. In the reported protocol, $[(CdSe)_{13}\ (octylamine)_{13}]$ lamellae can be retailored into $[(CdSe)_{13}\ (oleylamine)_{13}]$ via ligand-exchange by static soaking or successive sonication (Figure S1a−c), resulting in a reduction in scattering with small blue shifts (26−50 meV, Figure S1d), suggestive of effective ligand-exchange.[50−52] A full ligand-exchange process is also indicated by an increased interlayer spacing (2.6 → 4.6 nm in Figure S1e), which equals twice the chain length difference between octylamine and oleyamine.[30]

DOI: 10.1021/acs.chemmater.8b02468
Chem. Mater. 2018, 30, 5468−5477

Under HRTEM in Figure S2c, dot-like $(CdSe)_{13}$ clusters 1.6 nm in width are well-assembled inside of the 2D lamellae.[10,14] The uniform thickness of the 2D lamella is twice the estimated dimension (0.80 nm) of $(CdSe)_{13}$ predicted by XRD[30] and theoretical calculations.[53] This phenomenon for the aggregated $(CdSe)_{13}$ cannot be rationalized by variation of the isomerized morphology.

Repeated dilution and sonication processes of the ligand-exchanged $(CdSe)_{13}$ nanocluster yield a clear solution containing fully isolated nanoclusters suitable for size determination by SAXS analysis (Figure 3). An ellipsoid

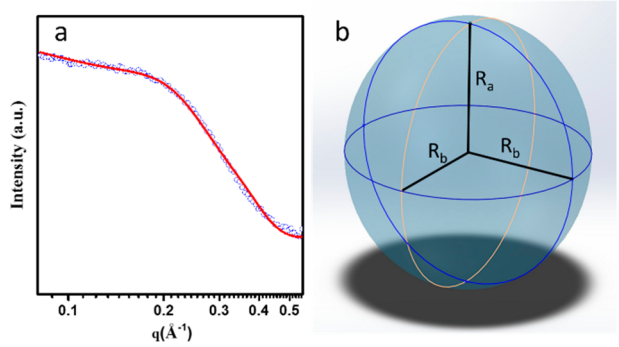

Figure 3. (a) SAXS pattern (line) with fitting results (dot) with (b) ellipsoid size model projection of $[(CdSe)_{13}\ (oleylamine)_{13}]$.

model with two radii (R_a, R_b) was rationally employed to fit the pattern, which gives rise to a single component of $[(CdSe)_{13}\ (oleylamine)_{13}]$ with two radii values that are numerically close (8.5 ± 0.002 and 8.1 ± 0.04 Å) in oleylamine−toluene solution. Such a dimension is twice the shortest dimension in all isomeric geometries of the theoretically proposed $(CdSe)_{13}$, as shown in Table 1. Further structural verification of $(CdSe)_{13}$ will be discussed and compared in the theoretical section.

Table 1. Relative Energies (in kcal/mol) of Bare or Ligand-Protected $(CdSe)_{13}$ Isomers[a]

Relative energies (kcal/mol)	cage-core	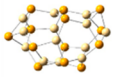 Cage	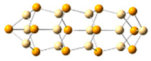 tubular
$(CdSe)_{13}$	0	11.43	33.76
$(CdSe)_{13}(MeNH_2)_{13}$	2.01	12.83	0
$(CdSe)_{13}(EtNH_2)_{13}$	3.29	12.76	0

[a]Results are calculated at the PBE0/SD-6-31G* level of theory. Solvation (in toluene) energy corrections are included by the PCM model with optimized gas-phase geometries.

Theoretical Modeling. On the basis of previously proposed isomer geometries,[2,53,54] three structures, denoted as cage-core (C_3), cage (C_1), and tubular (C_{3v}), are considered in this work. The theoretically calculated structures and relative energies for $(CdSe)_{13}$ isomers are shown in Table 1. The calculated relative energies for the bare clusters are consistent with those from previous computational studies,[2,54] i.e., the cage-core is the most stable structure whereas the tubular structure is the most unstable, with an energy difference as large as 34 kcal/mol. We then compute relative energies of these nanoclusters passivated by methylamines ($MeNH_2$) or ethylamines ($EtNH_2$) to mimic the experimental ligand passivation by octylamines or oleylamines. For the C_1 cage and C_{3v} tubular isomers, each Cd atom is ligated with one amine molecule. For the C_3 cage-core isomer, the one-to-one ligation geometry is not the most stable structure, and the four-coordinated structure is considered according to previous literature, i.e. 3, 7, and 3 of the Cd atoms are coordinated with 2, 1, and 0 ligands, respectively.[53,54] Surprisingly, while the relative stabilities between the cage-core and the cage isomers remain roughly the same scale upon ligand attachment, the tubular isomer is found to be dramatically stabilized by ligand passivation, to the extent that it becomes the lowest-energy structure.[34] Apparently, the energetics of the tubular structure is very dependent on the ligand environment. The energetic trend from L = $MeNH_2$ to $EtNH_2$ indicates that the stabilizing effect for the tubular isomer may increase with increasing length of the alkyl group, i.e., it is possible that the tubular isomer becomes considerably more stabilized than the cage-core structure with the actual ligand used in the experiment, the octylamines or oleylamines.

Ligand Stabilization Effect. The calculated binding energies are listed in Table 2. The ligand binding energies

Table 2. Ligand Binding Energy (E_b, kcal/mol) and Average Cd−N Bond Lengths (d_{Cd-N}, Å) of Different Ligand-Passivated $(CdSe)_{13}$ Isomers Computed by PBE0

Binding energy, kcal/mol (bond lengths, Å)	Cage-core	Cage	Tubular
L=$MeNH_2$	18.44 (2.41)	18.66 (2.41)	21.71 (2.37)
L=$EtNH_2$	18.39 (2.41)	18.63 (2.41)	21.71 (2.37)

are calculated by the equation $E_b = -\frac{1}{n}[E_{(CdSe)_{13}L_{13}} - (E_{(CdSe)_{13}} + nE_L)]$,[55] where n is the number of ligands (13 for these isomers), $E_{(CdSe)_{13}L_{13}}$ is the energy of the ligand-passivated cluster, and $E_{(CdSe)_{13}}$ and E_L are the total energies of the bare cluster and ligands, respectively. The average ligand binding energy of the ligand-passivated tubular isomer is about 3 kcal/mol higher than that of other isomers, corresponding to a slightly shorter optimized Cd−N bond length, d_{Cd-N} = 2.38 Å, with respect to d_{Cd-N} = 2.41 Å in other isomers. Note that the calculated Cd−N bond length in the tubular structure is very close to the value fitted by the EXAFS measurement, i.e., d_{Cd-N} = 2.37 Å.

Formation of Nanocluster Pairs. To compare with the experimentally measured HRTEM and SAXS results, we estimate the shape and size of $(CdSe)_{13}$ isomers based on the optimized structures and the covalent radii of the Cd and Se atoms.[56] The diameter of the $(CdSe)_{13}$ core in the roughly spherical cage-core structure is about 9.0 Å. The length and the diameter of the cylindrical tubular $(CdSe)_{13}$ are around 17.5 and 8.0 Å, respectively, in Figure 4. Apparently, there is a large

DOI: 10.1021/acs.chemmater.8b02468
Chem. Mater. 2018, 30, 5468−5477

discrepancy between the experimentally measured values with either structure.

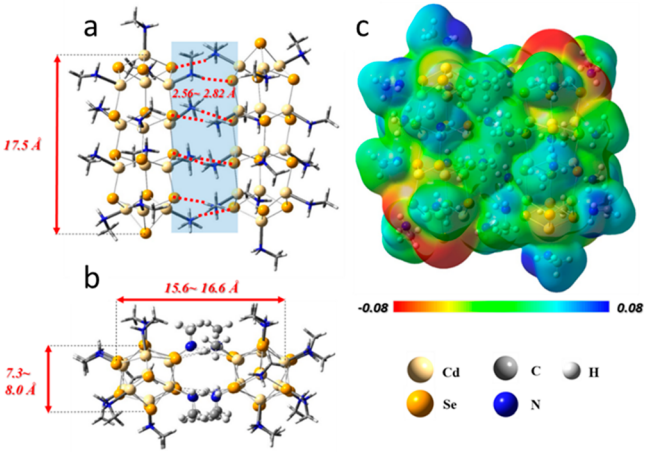

Figure 4. (a) Top view and (b) side view of the optimized structure of a $MeNH_2$ protected tubular $[(CdSe)_{13}]_2$ pair structure. The average bond length of the Se···H_N between neighboring tubes is around 2.6–2.8 Å. The theoretically calculated size parameters of the central metal core are also listed. (c) Electrostatic charges of the paired cluster showing the strong dipole–dipole interaction between the neighboring $(CdSe)_{13}$ tubes. The isovalue is 0.0004 electrons/Å^3, and the color represents the electrostatic potential ranging from −0.08 to 0.08 (in au).

In fact, the tubular structure not only has a much larger aspect ratio but is also directional, with one Se atom and one Cd atom positioned at each end of the long axis, implying a more uneven electron density distribution on the two terminals of the tube. This effect becomes the most striking when ligand passivation is involved. Without ligand attachment, the dipole moments of the bare cage-core and tubular isomers are similar (~5D, Table S2). However, with ligand passivation, as only one terminal (the Cd end) of the tubular isomer is coordinated by the amine, the dipole moment of the tubular isomer becomes significantly larger (~27 D, Table S2), pointing from the Se end (negative) to the Cd end (positive) along the tubular long axis. The Mulliken charge analysis reveals that the negative charges of the Se atoms significantly increase by 0.2–0.3 upon amine attachment, while the charges of the Cd atoms show only a slight variation within 0–0.15 (Table S3), suggesting a certain extent of electron transfer from N to Se through Cd. The dramatic dipole moment increase of the tubular isomer upon ligation may also be visualized by the electrostatic charges of the bare and $MeNH_2$-passivated structures (Figure S4).

In an organic solvent environment, the strong dipole–dipole interaction between two tubular monomers may lead to spontaneous pairing. Therefore, a paired-tubular structure formed by n antiparallel alignment of two tubular monomers, as shown in Figure 4, is considered and is found to be 26.40 kcal/mol (Table S4) more stable than two separated tubular monomers. The tubular pair leads to a much more stable structure, with the dipole moment largely diminished to only 0.62 D (Table S2). As the two monomers approach each other, the alkyl groups of the ligands in between rotate away from the other tube and stick out of the gap between the two monomers. In addition, one of the hydrogens on the amine group of one tube is found to point toward the Se atom of the other tube. As shown in Figure 4a,b, the distance between the Se and the hydrogen atom of the amines (H_N) in between is around 2.6–2.8 Å (marked by the red dotted lines in Figure 4a), much shorter than the average Se···H_N bond length in the monomer, 3.20 Å, indicative of the strong dipole driving force between the two tubular monomers.

It is evident that the shape and size of the tubular-pair structure are a lot more consistent with the experimental results. As shown in Figure 4, while the length (17.5 Å) and the thickness (~8.0 Å) of the paired cluster are close to those of the monomer, the width across the two monomers in the paired cluster is about 15.6–16.6 Å. Overall, the geometrical parameters of the tubular -pair are very consistent with the experimental value. In solid states, similar consecutive antiparallel coupling of $(CdSe)_{13}$ in the long lateral (side-by-side) and vertical (end-to-end) directions into an infinite 2D superlattice is also proposed (Figure S5), resulting in a sheet- or stripe-like 2D morphology as observed by HRTEM (Figure S2), which may further reduce the residual dipole moment. In the presence of a nonpolar solvent system with long alkyl chains, such a coupling shall become reversible, which leads to disassembling of $(CdSe)_{13}$ lamella back to dispersed cluster pairs (Figure S5).[10]

Chemical Bonding. Local bonding and chemical environments are verified by EXAFS (Figure 5) and magic-angle

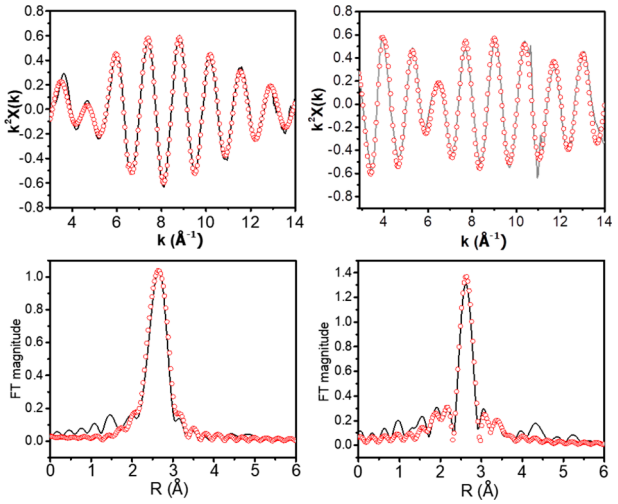

Figure 5. *k*- (upper) and *R*-space (bottom) fittings of the Cd K-edge (left) and Se K-edge (right) in $(CdSe)_{13}$ nanoclusters (experiment: line; fit: dots).

spinning (MAS) NMR (Figure 6). EXAFS, a powerful technique that resolves not only the interatomic distances but also the coordination numbers of adjacent atoms via X-ray backscattering signals,[40,57,58] is chosen over PDF to reveal local coordination information. On the basis of the Cd K-edge absorption fitting result, two distinguished bond lengths of Cd–N (2.365 ± 0.004 Å) and Cd–Se (2.621 ± 0.008 Å) are obtained, and the respective coordination numbers are determined to be 1.06 and 2.92, closely matching a four-coordinated Cd site. For the Se K-edge absorption, the first two shells suggest major components of Se–Cd (2.621 ± 0.007 Å) and a much longer Se–N (3.896 ± 0.004 Å), with individual coordination numbers optimally determined to be 2.92 and 3.56 (Table S1), respectively, indicative of additional N-backscattering to a three-coordinated Se site. In Figure S6, a

DOI: 10.1021/acs.chemmater.8b02468
Chem. Mater. 2018, 30, 5468–5477

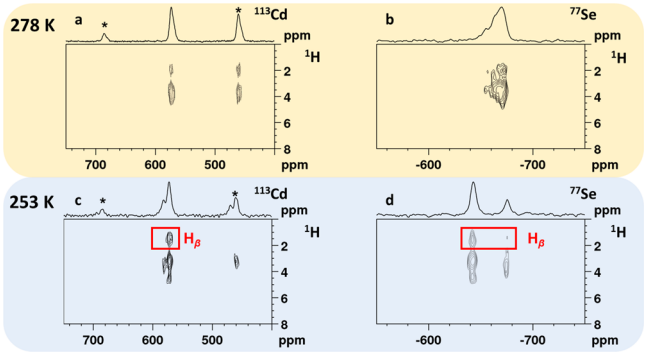

Figure 6. 2D HETCOR decoupled MAS NMR spectrum of (a,c) ^{113}Cd{^{1}H} and (b,d) ^{77}Se{^{1}H} of $(CdSe)_{13}(OA)_{13}$ nanoclusters conducted at 278 and 253 K. The spinning side-band patterns in the ^{113}Cd−^{1}H spectrum are labeled with asterisks. H_β proton signals are highlighted in red boxes.

paired cluster model with intercalated methylamines reveals this backscattering mechanism with multiple N−Se contributions. Such a complexity in the N chemical environment is also reflected by the inequivalent octylamines near the Se sites. Therefore, the second shell containing four inequivalent Se−N bonds can be rationalized by the paired cluster model (Figure S6). The C 1s, N 1s, Cd 3d, and Se 3d peaks are observed in X-ray photoelectron spectroscopy (XPS, Figure S7) and are deconvoluted into Gaussian components after subtracting the Shirley background. In $(CdSe)_{13}$, two main Cd binding energies, $3d_{5/2}$ and $3d_{3/2}$, centered at 404.8 and 411.6 eV, respectively, are slightly lower than the binding energies (405.2 and 411.9 eV) of Cd in phosphonic acid-capped CdSe QDs. On the other hand, two main Se binding energies, $3d_{5/2}$ and $3d_{3/2}$, centered at 53.0 and 53.9 eV, respectively, are significantly lower than the binding energies (54.1 and 54.6 eV) of Se in phosphonic acid-capped CdSe QDs.[59] In addition, the observation of two different N 1s binding energies indicates the coexistence of the amine and tertiary ammonium.[60] The XPS features of the Cd, Se, and N imply additional charge transfer from N in octylamines to Cd and to Se, especially from the terminal N to the terminal Se, resulting in dipole moment increase upon ligation (Figure S4), as predicted by the theoretical results (vide supra).

Further examination of the chemical environments of Cd, Se, and other elements is conducted by MAS NMR, which allows detection of proton interactions via heteronuclear correlation (HETCOR) experiments to understand bonding structures at variable temperatures. Surprisingly, both ^{77}Se (−667 ppm) and ^{113}Cd (574 ppm) NMR results reveal a relatively broad peak at 278 K (Figure 6), which splits into two peaks of ^{77}Se (−643, −675 ppm) and ^{113}Cd (573, 583 ppm) at 253 K (Figure 6). Upon cooling, the distance between the $(CdSe)_{13}$ cores is shortened, as indicated by a contration of d_{002} by 4.3% (or 0.56 Å, Figure S8), indicating stronger confinement of the intercalated octylamines. Such an intercalated structure of octylamines between the $(CdSe)_{13}$ clusters induces split chemical shifts for both Cd and Se at 253 K, similar to the temperature-dependent dynamics of the lithium intercalation in $Li_3Al_xTi_{2-x}(PO_4)_3$ and $Li_7La_3Zr_2O_{12}$ (LLZO).[61,62] Further deconvolution of ^{77}Se and ^{113}Cd MAS NMR spectra results in two peaks with an intensity ratio around 4:9 for both elements (Figure S10), indicative of two distinct chemical environments in solid states. Previous theoretical models were unable to explain such a phenomenon unless an intermolecular proton coupling was included, forming different types of interaction geometries on the surfaces of $(CdSe)_{13}$.[54]

To explore this phenomenon, HETCOR experiments of ^{15}N{^{1}H}, ^{77}Se{^{1}H}, ^{113}Cd{^{1}H}, and ^{13}C{^{1}H} were conducted at two temperatures (Figures 6 and S10). Spatial correlations between C_α (C_1) protons (~3.6 ppm) and NH_2 protons (8.7, 9.9 ppm) were observed by ^{15}N{^{1}H} HETCOR experiments (Figure S11), confirming moieties of octylamines. At 278 K, both selenium and cadmium showed spatial correlations with H_α and H_β (Figure 6). When the temperature was lowered to 253 K, unique H_β features (1.2−2.4 ppm in Figure 6) could be distinguished via ^{77}Se{^{1}H} and ^{113}Cd{^{1}H} HETCOR experiments, also confirming two types of Cd and Se. The results of MAS NMR and HETCOR experiments indicate that around 9 out of 13 Cd or Se atoms have explicit spatial correlations with the H_β atoms, while the other 4 Cd or Se atoms do not. A

Table 3. Summary of the Theoretically Predicted and the Experimentally Observed Parameters of Different Geometry Models of the $(CdSe)_{13}$ MSCs[a]

Structural Parameters / Geometry Models	Total Energy (kcal/mol)	Size (Å)	Bond Length (Å)	Type of Cd/Se by NMR	Number of Atoms Showing H_β Interaction
Cage-Core monomer	Relatively unstable with ligation	11.2 Å x 11.3 Å	Cd-Se: 2.67 ± 0.05Å Cd-N: 2.41 ± 0.03Å	1 Cd type 2 Se types (ratio 1 : 12)	13 Cd and 12 Se
Tubular monomer	More stable with ligation	8.0Å x 17.0 Å	Cd-Se: 2.69 ± 0.03Å **Cd-N: 2.37 ± 0.02Å**	1 Cd type 1 Se type	13 Cd and 13 Se
Tubular pairs	**Most stable upon coupling**	**16.5Å x 17.0 Å**	Cd-Se: 2.69 ± 0.03Å **Cd-N: 2.37 ± 0.02Å**	**2 Cd & 2 Se types (ratio 4:9)**	**9 Cd and 9 Se**
		SAXS: **16.2Å x 17.0Å**	**EXAFS:** Cd-Se: 2.62 ± 0.01Å **Cd-N: 2.37 ± 0.01Å**	**MAS NMR:** **2 Cd & 2 Se types (ratio 4:8.3 & 4:8.7)**	**HETCOR:** **9 Cd and 9 Se**

[a]The theoretical and experimental data are presented in black and red, respectively.

DOI: 10.1021/acs.chemmater.8b02468
Chem. Mater. 2018, 30, 5468−5477

similar spatial correlation between the ligands and surface Se sites have been observed in 2 nm CdSe nanoparticles.[38]

Close inspection of the proposed paired cluster geometry reveals the origin of the 4:9 ratio observed in the NMR spectra (Figure S9). When the two clusters approach each other, the intercalated octylamines stick out of the gap between the two monomers and stretch away from the $(CdSe)_{13}$ surface. As a result, the four Cd atoms ligated with intercalating octylamines, as well as the four Se atoms on the bridging-face of the $(CdSe)_{13}$, do not show spatial interactions with H_β. In contrast, the nine Cd atoms ligated with the peripheral octylamines, as well as the peripheral Se atoms, may show stronger H_β interaction as the floppy alkyl chain may wiggle to the proximity of the $(CdSe)_{13}$ tube surface (Figure S9). The presence of two chemical environments for Cd and Se as well as their relative correlations with H_β observed by NMR provide further evidence of $(CdSe)_{13}$ coupling into pairs, complementary to the paired cluster model revealed by HRETM, SAXS, DFT, and EXAFS, as shown in Table 3.

Optoelectronic Spectrum. TDDFT calculations are performed in an attempt to interpret the measured absorption spectra. It is well-known that theoretical evaluation for the absolute values of the absorption peaks for these nanoclusters is not a trivial task, and the results strongly depend on the chosen functional and the basis set,[35] as shown in Tables S5 and S6. Nevertheless, the calculated relative energies and intensities between the first few low-energy absorption peaks could serve as a good reference to the experimental spectra.[63] On the basis of the energy calculations and the size analysis, we compute the absorption spectra of the tubular monomer and the paired cluster, as shown in Figure S13. Both spectra have to be blue-shifted by around 0.35 eV in order to be compared with the experimental absorption spectra, but both show a larger oscillator strength for the lowest-energy peak than the second lowest one, consistent with the relative absorbance measured experimentally. Within the energy range from 3.0 to 3.5 eV, the calculated monomer spectrum shows major absorption peaks at 3.12 (S_1), 3.30 (S_2 and S_3), and 3.45 eV (S_4 and S_5); the calculated paired cluster spectrum shows major absorption peaks at 3.21 (S_1 and S_2), 3.32 (S_3 and S_4), and 3.43 eV (S_7) (Tables S5 and S6). The first few optical transitions for the monomer and the paired cluster are extremely close in energy. This can be understood from the frontier orbital analysis, as shown in Figure S14. Consistent with the dipole moment distribution of the tubular monomer, the HOMO and the LUMO of the tubular monomer are concentrated on the Se end and the Cd end, respectively, as shown in Figure S14. The molecular orbital transition for the S_1 state of the tubular monomer is dominated by a HOMO to LUMO transition, a strong charge transfer excitation. Similarly, the S_1 (or S_2) state of the tubular paired clusters may be roughly characterized as a dual charge transfer excitation from the HOMO (or HOMO−1) to LUMO, distributed on the two Se ends and two Cd ends, respectively.

Note that the two CdSe cores in the pair are not strucurally merged and remain fully separated by ligands. Therefore, the usual red shift predicted by the quantum confinement effect does not apply. With a 4−5 Å distance between the two tubular cores, the delocalization of the frontier orbitals on one tube into its neighbor is negligible; thus, the energy difference between the frontier orbitals of the monomer and those of the paired cluster is very small. As the two tubes are paired, the HOMO (and HOMO−1) remains about the same energy as in the monomer (Figure S14), but the LUMO becomes slightly more spread-out and is destabilized by about 0.1 eV, leading to a minute blue shift of the first excitation peak from monomer to the cluster pair. Hence, the calculated optical transition energies for the monomer and the paired cluster are almost indistinguishable.

CONCLUSIONS

A paired cluster model for $(CdSe)_{13}$ is proposed and supported via nondestructive characterization tools and DFT calculations. In this study, structural and phase transformations during formation of $(CdSe)_{13}$ bilayers are verified by X-ray scattering (SAXS and WAXS) and diffraction (XRD) techniques. Electron microscopy (TEM) reveals a 2D morphology of $(CdSe)_{13}$ aggregates after a long recrystallization process. The local chemical bonding and environments are established based on XPS, EXAFS, and MAS NMR results. The coordination of Cd remains four (three Se and one N), while the coordination of Se involves additional N-back-scattering from the octylamine intercalated between two adjacent $(CdSe)_{13}$ clusters. Quantitative analyses of both SAXS and DFT suggest an ellipsoid-shaped nanocluster consisting of two coupled $(CdSe)_{13}$ tubular monomers, different from the previously proposed cage-core single-nanocluster model. Both the size and shape of the paired nanocluster as well as the underlying dipole−dipole interaction mechanism of the spontaneous pairing are fully supported by theoretical calculations. The paired nanocluster model established by theoretical and experimental evidence offers a more thorough understanding of II−VI semiconductor nanoclusters as well as insights on sequential growth into 2D materials.

EXPERIMENTAL SECTION

Chemicals. *n*-Octylamine (*n*-OA) was obtained from ACROS (+99%), selenourea (98%, metal basis) from Sigma-Aldrich, $Cd(OAc)_2{\cdot}2H_2O$ from ACROS, trioctylphosphine (TOP) from ACROS (90%), and oleylamine (or *cis*-9-octadecenylamine) from ACROS (80−90%). All were used as received and stored under N_2. Toluene from TEDIA (Absolv) was purged with dry N_2 for at least 1 h and stored under N_2 prior to use.

Synthesis of [$(CdSe)_{13}$(*n*-octylamine)$_{13}$]. All synthetic and purification procedures were conducted in a glovebox with some modification procedure according to previous literature.[10] Cadmium acetate dihydrate [$Cd(OAc)_2{\cdot}2H_2O$] (80 mg, 0.30 mmol) was dissolved in *n*-OA (6.7 g, 0.052 mol) in a reaction bottle and heated in a 65 °C oil bath for 1 h. Selenourea (67 mg, 0.54 mmol) was dissolved in *n*-OA (2.8 g, 0.022 mol) in the glovebox, and a pale-red solution was normally obtained. As the color of the selenourea solution changed to deep red, the precursor solution was quickly injected into the $Cd(OAc)_2$−OA solution at room temperature (20−25 °C) with stirring. During the first 2 h, the reaction mixture underwent a noticable color change from colorless (0 min) to a cloudy greenish-yellow. After another 24−72 h in N_2, the precipitate turned white under a light-red supernatant. The reaction mixture was subsequently heated at 80 °C in an oil bath for another 1 h. During this time, the supernatant turned dark red and the precipitate remained white. A small amount of black or gray solids known as byproducts and the red supernatant were subsequently converted to colorless TOP═Se after injection of TOP (90%, 0.5−1.0 mL), whereupon the precipitate was ready for storage as TOP-purified [$(CdSe)_{13}$(*n*-OA)$_{13}$]. The white precipitate was collected via a benchtop centrifuge (6000 rpm) for 5−10 min, and the colorless supernatant was discarded. The final product was obtained after repeating this purification process 5−6 times using an OA−toluene solution (10 mL, 5−10% w/w in toluene) to remove TOP═Se. N_2-

DOI: 10.1021/acs.chemmater.8b02468
Chem. Mater. 2018, 30, 5468−5477

dried toluene could be used in the last few purification cycles to remove trace amounts of adsorbed OA. The resulting product was unstable toward exposure of polar solvent or upon drying. The residual toluene was removed in vacuum, leaving $[(CdSe)_{13}(n\text{-}OA)_{13}]$ as a white or partially red slushy solid. Anal. Calcd for $[(CdSe)_{13}(n\text{-}OA)_{13}]$: C, 29.97; H, 5.97; N, 4.37. Found, C, 32.35; H, 6.26; N, 4.70. All values are given in percentages. UV−vis (toluene) E_{max}, eV: 3.95, 3.65, 3.49. To preserve $[(CdSe)_{13}(n\text{-}OA)_{13}]$, the $[(CdSe)_{13}(n\text{-}OA)_{13}]$ was always stored in the TOP mixture under N_2 conditions, and aliquots of this mixture were purified in above procedures as needed.

Isolation of $[(CdSe)_{13}$(oleylamine)$_{13}]$ via Ligand-Exchange. All synthetic procedures were conducted in a drybox with some modification according to previous literature.[10] An aliquot (ca. 0.5 mL, 1.1×10^{-2} mmol of $[(CdSe)_{13}(n\text{-}OA)_{13}]$) from the TOP-purified $[(CdSe)_{13}(n\text{-}OA)_{13}]$ was collected by the purification process mentioned above and then redispersed in 10 mL of toluene. Then, 0.5 mL of the $(CdSe)_{13}(n\text{-}OA)_{13}$−toluene solution was added into as-received OA (yellow, 15 mL) with slight shaking to produce a dispersion of the $(CdSe)_{13}(n\text{-}OA)_{13}$. The suspension was prepared at room temperature without stirring for 1 week or even longer. In the first 2 days, the white precipitate remained at the bottom of the flask, as bundled $[(CdSe)_{13}(n\text{-}OA)_{13}]$. As ligand-exchange proceeded, the precipitate gradually diminished, eventually leaving a transparent solution with a trace amount of white slush. After more than 1 week, the mixture was diluted with toluene and centrifuged (7500 rpm, 30 min), and the pale-yellow supernatant was discarded. The resulting white precipitate was washed with toluene (5 mL), the mixture slush centrifuged, and the supernatant discarded. This purification process was repeated several times. Eventually, the ligand-exchanged $(CdSe)_{13}(OA)_{13}$ was redisolved in toluene as a homogeneous solution. UV−vis (toluene) E_{max}, eV: 3.99, 3.66, 3.52.

Characterization. The electron microscope images were obtained using a Hitachi H-7100 (TEM) and FEI Tecnai G2 (HRTEM) located in the Instrumentation Center of National Taiwan University (NTU), Taipei, Taiwan. Synchrotron-based powder XRD measurement was conducted in the National Synchrotron Radiation Research Center (NSRRC, Taiwan), TLS-01C2/TPS-09A experiment station equipped with an 18/15 keV (λ = 0.0689/0.0826 nm) diffraction beam energy. Capillary samples were placed in a rotatory goniometer that eliminates preferred orientation during data collection. All small/wide-angle X-ray scattering (SAXS/WAXS) experiments were operated on the NSRRC, 23A experiment station with energy = 15 keV. SAXS data was fitted by IGOR; the SLD is offered by the NIST Center for Neutron Research. The XPS spectra were obtained using the VG Scientific Microlab 350 located in the Instrumentation Center of National Chiao Tung University (NCTU), Hsinchu, Taiwan. All solid-state decoupled NMR experiments were carried out on a wide-bore 14.1 T Bruker Avance III spectrometer equipped with a 3.2 mm MAS probe head in NTU. The Larmor frequencies for ^{1}H, ^{13}C, ^{15}N, ^{77}Se, and ^{113}Cd were 600.21, 150.93, 60.82, 114.39, and 133.12 MHz, respectively. The sample was spun at 15 kHz. For all CP schemes, the ^{1}H RF field was set as 50 kHz, and the RF field for ^{13}C, ^{15}N, ^{77}Se, and ^{113}Cd channels linearly ramped from 80 to 100% in strength and was set to maximize the signal intensity. The contact time for ^{13}C and ^{15}N CP was 200 μs, and the contact time for ^{77}Se and ^{113}Cd CP was 500 μs. The recycle delay was 3 s. For all CP-HETCOR experiments, ^{1}H frequency-switching Lee−Goburg (FSLG) homonuclear decoupling at a RF field strength of 90 kHz was applied during t_1 evolution. The EXAFS experiment was operated in the NSRRC, 01C experiment station with X-ray energy range = 6−33 keV. All EXAFS data was analyzed by FEFF7.0 to operate energy calibration and curve fitting.

Computational Details. Density functional theory (DFT) and time-dependent density functional theory (TDDFT) calculations of all clusters were carried out by the Gaussian 09 program.[64] The ground-state geometry of the CdSe clusters was optimized with the PBE0[65,66] functional and the SD-6-31G* basis set, in which the Stuttgart/Dresden (SD) basis set and ECP[67−70] are adopted for the Cd and Se atom, and the 6-31G*[71,72] was used for the main group ligand atoms. The minima were confirmed with no imaginary frequencies. The solvent (toluene, ε = 2.3741) corrections were included on top of the gas-phase optimized geometry with the polarizable continuum model (PCM).[73] TDDFT calculations[74] based on the optimized structures at ground states were performed using the PBE0 functional and the same basis set and pseudopotential as those mentioned above.

■ ASSOCIATED CONTENT

Supporting Information

The Supporting Information is available free of charge on the ACS Publications website at DOI: 10.1021/acs.chemmater.8b02468.

UV−vis absorption spectra, XRD patterns, TEM/HRTEM images, solid-state NMR and HETCOR spectra, SAXS spectrum and fitting results, XPS spectra, EXAFS fitting results, Raman spectrum, electrostatic charges of $(CdSe)_{13}$, TDDFT spectra, Mulliken charge analysis results, illustrations of self-assembly, and calculated frontier orbitals of $(CdSe)_{13}$ (PDF)

■ AUTHOR INFORMATION

Corresponding Authors

*E-mail: eliseytli@ntnu.edu.tw (E.Y.L.).
*E-mail: yliu@ntnu.edu.tw (Y.-H.L.).

ORCID

Yi-Qi Yeh: 0000-0002-2387-3600
Elise Y. Li: 0000-0003-1206-1110
Yi-Hsin Liu: 0000-0001-7069-4536

Author Contributions

‖T.-E.H., T.-W.Y., and C.-Y.H. contributed equally.

Notes

The authors declare no competing financial interest.

■ ACKNOWLEDGMENTS

This research is supported by National Taiwan Normal University and the Taiwan Ministry of Science and Technology under contract No.103-2113-M-003-011-MY2, 105-2113-M-003-006-MY2 and 106-2113-M-003-010-MY3. The authors thank Dr. T. S. Chang (TLS-01C1, EXAFS), Dr. C. K. Chang (TLS-01C2, XRD) and Dr. Y. C. Chuang (TPS-09A, 90K XRD) at National Synchrotron Radiation Research Center for helpful assistance in those measurements.

■ REFERENCES

(1) Kasuya, A.; Sivamohan, R.; Barnakov, Y. A.; Dmitruk, I. M.; Nirasawa, T.; Romanyuk, V. R.; Kumar, V.; Mamykin, S. V.; Tohji, K.; Jeyadevan, B.; Shinoda, K.; Kudo, T.; Terasaki, O.; Liu, Z.; Belosludov, R. V.; Sundararajan, V.; Kawazoe, Y. Ultra-stable nanoparticles of CdSe revealed from mass spectrometry. *Nat. Mater.* **2004**, *3*, 99−102.

(2) Nguyen, K. A.; Day, P. N.; Pachter, R. Understanding Structural and Optical Properties of Nanoscale CdSe Magic-Size Quantum Dots: Insight from Computational Prediction. *J. Phys. Chem. C* **2010**, *114*, 16197−16209.

(3) Joo, J.; Son, J. S.; Kwon, S. G.; Yu, J. H.; Hyeon, T. Low-Temperature Solution-Phase Synthesis of Quantum Well Structured CdSe Nanoribbons. *J. Am. Chem. Soc.* **2006**, *128*, 5632−5633.

(4) Grebinski, J. W.; Hull, K. L.; Zhang, J.; Kosel, T. H.; Kuno, M. Solution-Based Straight and Branched CdSe Nanowires. *Chem. Mater.* **2004**, *16*, 5260−5272.

(5) Kim, S.; Fisher, B.; Eisler, H.-J.; Bawendi, M. Type-II Quantum Dots: CdTe/CdSe(Core/Shell) and CdSe/ZnTe(Core/Shell) Heterostructures. *J. Am. Chem. Soc.* **2003**, *125*, 11466−11467.

DOI: 10.1021/acs.chemmater.8b02468
Chem. Mater. 2018, 30, 5468−5477

(6) Peng, X.; Schlamp, M. C.; Kadavanich, A. V.; Alivisatos, A. P. Epitaxial Growth of Highly Luminescent CdSe/CdS Core/Shell Nanocrystals with Photostability and Electronic Accessibility. *J. Am. Chem. Soc.* **1997**, *119*, 7019−7029.
(7) Peng, Z. A.; Peng, X. Formation of High-Quality CdTe, CdSe, and CdS Nanocrystals Using CdO as Precursor. *J. Am. Chem. Soc.* **2001**, *123*, 183−184.
(8) Murray, C. B.; Norris, D. J.; Bawendi, M. G. Synthesis and characterization of nearly monodisperse CdE (E = sulfur, selenium, tellurium) semiconductor nanocrystallites. *J. Am. Chem. Soc.* **1993**, *115*, 8706−8715.
(9) Harrell, S. M.; McBride, J. R.; Rosenthal, S. J. Synthesis of Ultrasmall and Magic-Sized CdSe Nanocrystals. *Chem. Mater.* **2013**, *25*, 1199−1210.
(10) Wang, Y.; Liu, Y.-H.; Zhang, Y.; Wang, F.; Kowalski, P. J.; Rohrs, H. W.; Loomis, R. A.; Gross, M. L.; Buhro, W. E. Isolation of the Magic-Size CdSe Nanoclusters [(CdSe)13(n-octylamine)13] and [(CdSe)13(oleylamine)13]. *Angew. Chem., Int. Ed.* **2012**, *51*, 6154−6157.
(11) Gary, D. C.; Terban, M. W.; Billinge, S. J. L.; Cossairt, B. M. Two-Step Nucleation and Growth of InP Quantum Dots via Magic-Sized Cluster Intermediates. *Chem. Mater.* **2015**, *27*, 1432−1441.
(12) Schliehe, C.; Juarez, B. H.; Pelletier, M.; Jander, S.; Greshnykh, D.; Nagel, M.; Meyer, A.; Foerster, S.; Kornowski, A.; Klinke, C.; Weller, H. Ultrathin PbS Sheets by Two-Dimensional Oriented Attachment. *Science* **2010**, *329*, 550−553.
(13) Riedinger, A.; Ott, F. D.; Mule, A.; Mazzotti, S.; Knusel, P. N.; Kress, S. J. P.; Prins, F.; Erwin, S. C.; Norris, D. J. An intrinsic growth instability in isotropic materials leads to quasi-two-dimensional nanoplatelets. *Nat. Mater.* **2017**, *16*, 743−748.
(14) Liu, Y.-H.; Wang, F.; Wang, Y.; Gibbons, P. C.; Buhro, W. E. Lamellar Assembly of Cadmium Selenide Nanoclusters into Quantum Belts. *J. Am. Chem. Soc.* **2011**, *133*, 17005−17013.
(15) Liu, Y.; Zhang, B.; Fan, H.; Rowell, N.; Willis, M.; Zheng, X.; Che, R.; Han, S.; Yu, K. Colloidal CdSe 0-Dimension Nanocrystals and Their Self-Assembled 2-Dimension Structures. *Chem. Mater.* **2018**, *30*, 1575−1584.
(16) Qi, H.; Yu, P.; Wang, Y.; Han, G.; Liu, H.; Yi, Y.; Li, Y.; Mao, L. Graphdiyne Oxides as Excellent Substrate for Electroless Deposition of Pd Clusters with High Catalytic Activity. *J. Am. Chem. Soc.* **2015**, *137*, 5260−5263.
(17) Wang, Y.; Fedin, I.; Zhang, H.; Talapin, D. V. Direct optical lithography of functional inorganic nanomaterials. *Science* **2017**, *357*, 385.
(18) Soloviev, V. N.; Eichhöfer, A.; Fenske, D.; Banin, U. Molecular Limit of a Bulk Semiconductor: Size Dependence of the "Band Gap" in CdSe Cluster Molecules. *J. Am. Chem. Soc.* **2000**, *122*, 2673−2674.
(19) Kudera, S.; Zanella, M.; Giannini, C.; Rizzo, A.; Li, Y.; Gigli, G.; Cingolani, R.; Ciccarella, G.; Spahl, W.; Parak, W. J.; Manna, L. Sequential Growth of Magic-Size CdSe Nanocrystals. *Adv. Mater.* **2007**, *19*, 548−552.
(20) Soloviev, V. N.; Eichhöfer, A.; Fenske, D.; Banin, U. Size-Dependent Optical Spectroscopy of a Homologous Series of CdSe Cluster Molecules. *J. Am. Chem. Soc.* **2001**, *123*, 2354−2364.
(21) Wang, Y.; Zhang, Y.; Wang, F.; Giblin, D. E.; Hoy, J.; Rohrs, H. W.; Loomis, R. A.; Buhro, W. E. The Magic-Size Nanocluster (CdSe)34 as a Low-Temperature Nucleant for Cadmium Selenide Nanocrystals; Room-Temperature Growth of Crystalline Quantum Platelets. *Chem. Mater.* **2014**, *26*, 2233−2243.
(22) Pradhan, N.; Xu, H.; Peng, X. Colloidal CdSe Quantum Wires by Oriented Attachment. *Nano Lett.* **2006**, *6*, 720−724.
(23) Liu, Y.-H.; Wayman, V. L.; Gibbons, P. C.; Loomis, R. A.; Buhro, W. E. Origin of High Photoluminescence Efficiencies in CdSe Quantum Belts. *Nano Lett.* **2010**, *10*, 352−357.
(24) Yu, J. H.; Liu, X.; Kweon, K. E.; Joo, J.; Park, J.; Ko, K.-T.; Lee, D. W.; Shen, S.; Tivakornsasithorn, K.; Son, J. S.; Park, J.-H.; Kim, Y.-W.; Hwang, G. S.; Dobrowolska, M.; Furdyna, J. K.; Hyeon, T. Giant Zeeman splitting in nucleation-controlled doped CdSe:Mn2+ quantum nanoribbons. *Nat. Mater.* **2010**, *9*, 47.
(25) Vlaskin, V. A.; Barrows, C. J.; Erickson, C. S.; Gamelin, D. R. Nanocrystal Diffusion Doping. *J. Am. Chem. Soc.* **2013**, *135*, 14380−14389.
(26) Yang, J.; Fainblat, R.; Kwon, S. G.; Muckel, F.; Yu, J. H.; Terlinden, H.; Kim, B. H.; Iavarone, D.; Choi, M. K.; Kim, I. Y.; Park, I.; Hong, H.-K.; Lee, J.; Son, J. S.; Lee, Z.; Kang, K.; Hwang, S.-J.; Bacher, G.; Hyeon, T. Route to the Smallest Doped Semiconductor: Mn2+-Doped (CdSe)13 Clusters. *J. Am. Chem. Soc.* **2015**, *137*, 12776−12779.
(27) Muckel, F.; Yang, J.; Lorenz, S.; Baek, W.; Chang, H.; Hyeon, T.; Bacher, G.; Fainblat, R. Digital Doping in Magic-Sized CdSe Clusters. *ACS Nano* **2016**, *10*, 7135−7141.
(28) Yu, K. CdSe Magic-Sized Nuclei, Magic-Sized Nanoclusters and Regular Nanocrystals: Monomer Effects on Nucleation and Growth. *Adv. Mater.* **2012**, *24*, 1123−1132.
(29) Beecher, A. N.; Yang, X.; Palmer, J. H.; LaGrassa, A. L.; Juhas, P.; Billinge, S. J. L.; Owen, J. S. Atomic Structures and Gram Scale Synthesis of Three Tetrahedral Quantum Dots. *J. Am. Chem. Soc.* **2014**, *136*, 10645−10653.
(30) Wang, Y.; Liu, Y.-H.; Zhang, Y.; Kowalski, P. J.; Rohrs, H. W.; Buhro, W. E. Preparation of Primary Amine Derivatives of the Magic-Size Nanocluster (CdSe)13. *Inorg. Chem.* **2013**, *52*, 2933−2938.
(31) Das, A.; Liu, C.; Byun, H. Y.; Nobusada, K.; Zhao, S.; Rosi, N.; Jin, R. Structure Determination of [Au18(SR)14]. *Angew. Chem., Int. Ed.* **2015**, *54*, 3140−3144.
(32) Wilcoxon, J. P.; Abrams, B. L. Synthesis, structure and properties of metal nanoclusters. *Chem. Soc. Rev.* **2006**, *35*, 1162−1194.
(33) Hua, X.; Liu, Z.; Bruce, P. G.; Grey, C. P. The Morphology of TiO2 (B) Nanoparticles. *J. Am. Chem. Soc.* **2015**, *137*, 13612−13623.
(34) Nguyen, K. A.; Pachter, R.; Day, P. N. Computational Prediction of Structures and Optical Excitations for Nanoscale Ultrasmall ZnS and CdSe Clusters. *J. Chem. Theory Comput.* **2013**, *9*, 3581−3596.
(35) Del Ben, M.; Havenith, R. W. A.; Broer, R.; Stener, M. Density Functional Study on the Morphology and Photoabsorption of CdSe Nanoclusters. *J. Phys. Chem. C* **2011**, *115*, 16782−16796.
(36) Huang, X.; Li, J.; Zhang, Y.; Mascarenhas, A. From 1D Chain to 3D Network: Tuning Hybrid II-VI Nanostructures and Their Optical Properties. *J. Am. Chem. Soc.* **2003**, *125*, 7049−7055.
(37) Li, T.; Senesi, A. J.; Lee, B. Small Angle X-ray Scattering for Nanoparticle Research. *Chem. Rev.* **2016**, *116*, 11128−11180.
(38) Berrettini, M. G.; Braun, G.; Hu, J. G.; Strouse, G. F. NMR Analysis of Surfaces and Interfaces in 2-nm CdSe. *J. Am. Chem. Soc.* **2004**, *126*, 7063−7070.
(39) Tian, L.-J.; Peng, Y.; Chen, D.-L.; Ma, J.-Y.; Yu, H.-Q.; Li, W.-W. Spectral insights into the transformation and distribution of CdSe quantum dots in microorganisms during food-chain transport. *Sci. Rep.* **2017**, *7*, 4370.
(40) Aruguete, D. M.; Marcus, M. A.; Li, L.-s.; Williamson, A.; Fakra, S.; Gygi, F.; Galli, G. A.; Alivisatos, A. P. Surface Structure of CdSe Nanorods Revealed by Combined X-ray Absorption Fine Structure Measurements and ab Initio Calculations. *J. Phys. Chem. C* **2007**, *111*, 75−79.
(41) Cossairt, B. M.; Owen, J. S. CdSe Clusters: At the Interface of Small Molecules and Quantum Dots. *Chem. Mater.* **2011**, *23*, 3114−3119.
(42) Demortière, A.; Schaller, R. D.; Li, T.; Chattopadhyay, S.; Krylova, G.; Shibata, T.; dos Santos Claro, P. C.; Rowland, C. E.; Miller, J. T.; Cook, R.; Lee, B.; Shevchenko, E. V. In Situ Optical and Structural Studies on Photoluminesence Quenching in CdSe/CdS/Au Heterostructures. *J. Am. Chem. Soc.* **2014**, *136*, 2342−2350.
(43) Dukes, A. D.; McBride, J. R.; Rosenthal, S. J. Synthesis of Magic-Sized CdSe and CdTe Nanocrystals with Diisooctylphosphinic Acid. *Chem. Mater.* **2010**, *22*, 6402−6408.
(44) Guo, S.; Konopny, L.; Popovitz-Biro, R.; Cohen, H.; Porteanu, H.; Lifshitz, E.; Lahav, M. Thioalkanoates as Site-Directing Nucleating Centers for the Preparation of Patterns of CdS

DOI: 10.1021/acs.chemmater.8b02468
Chem. Mater. 2018, 30, 5468−5477

Nanoparticles within 3-D Crystals and LB Films of Cd Alkanoates. *J. Am. Chem. Soc.* **1999**, *121*, 9589−9598.
(45) Son, J. S.; Wen, X. D.; Joo, J.; Chae, J.; Baek, S. i.; Park, K.; Kim, J. H.; An, K.; Yu, J. H.; Kwon, S. G.; Choi, S. H.; Wang, Z.; Kim, Y. W.; Kuk, Y.; Hoffmann, R.; Hyeon, T. Large-Scale Soft Colloidal Template Synthesis of 1.4 nm Thick CdSe Nanosheets. *Angew. Chem., Int. Ed.* **2009**, *48*, 6861−6864.
(46) Huang, X.; Parashar, V. K.; Gijs, M. A. M. Synergistic effect of carboxylic and amine ligands on the synthesis of CdSe nanocrystals. *RSC Adv.* **2016**, *6*, 88911−88915.
(47) Webber, D. H.; Buckley, J. J.; Antunez, P. D.; Brutchey, R. L. Facile dissolution of selenium and tellurium in a thiol-amine solvent mixture under ambient conditions. *Chem. Sci.* **2014**, *5*, 2498−2502.
(48) Heeley, E. L.; Hughes, D. J.; El Aziz, Y.; Williamson, I.; Taylor, P. G.; Bassindale, A. R. Properties and self-assembled packing morphology of long alkyl-chained substituted polyhedral oligomeric silsesquioxanes (POSS) cages. *Phys. Chem. Chem. Phys.* **2013**, *15*, 5518−5529.
(49) Greaves, T.; Broomhall, H.; Weerawardena, A.; Osborne, D. A.; Canonge, B. A.; Drummond, C. J. How ionic species structure influences phase structure and transitions from protic ionic liquids to liquid crystals to crystals. *Faraday Discuss.* **2018**, *206*, 29−48.
(50) Luo, X.; Liu, P.; Truong, N. T. N.; Farva, U.; Park, C. Photoluminescence Blue-Shift of CdSe Nanoparticles Caused by Exchange of Surface Capping Layer. *J. Phys. Chem. C* **2011**, *115*, 20817−20823.
(51) Dirin, D. N.; Dreyfuss, S.; Bodnarchuk, M. I.; Nedelcu, G.; Papagiorgis, P.; Itskos, G.; Kovalenko, M. V. Lead Halide Perovskites and Other Metal Halide Complexes As Inorganic Capping Ligands for Colloidal Nanocrystals. *J. Am. Chem. Soc.* **2014**, *136*, 6550−6553.
(52) Frederick, M. T.; Weiss, E. A. Relaxation of Exciton Confinement in CdSe Quantum Dots by Modification with a Conjugated Dithiocarbamate Ligand. *ACS Nano* **2010**, *4*, 3195−3200.
(53) Sangthong, W.; Limtrakul, J.; Illas, F.; Bromley, S. T. Persistence of magic cluster stability in ultra-thin semiconductor nanorods. *Nanoscale* **2010**, *2*, 72−77.
(54) Azpiroz, J. M.; Matxain, J. M.; Infante, I.; Lopez, X.; Ugalde, J. M. A DFT/TDDFT study on the optoelectronic properties of the amine-capped magic (CdSe)13 nanocluster. *Phys. Chem. Chem. Phys.* **2013**, *15*, 10996−11005.
(55) Gao, Y.; Zhou, B.; Kang, S.-g.; Xin, M.; Yang, P.; Dai, X.; Wang, Z.; Zhou, R. Effect of ligands on the characteristics of (CdSe)13 quantum dots. *RSC Adv.* **2014**, *4*, 27146−27151.
(56) Sanville, E.; Burnin, A.; BelBruno, J. J. Experimental and Computational Study of Small (n = 1−16) Stoichiometric Zinc and Cadmium Chalcogenide Clusters. *J. Phys. Chem. A* **2006**, *110*, 2378−2386.
(57) Rockenberger, J.; Tröger, L.; Kornowski, A.; Vossmeyer, T.; Eychmüller, A.; Feldhaus, J.; Weller, H. EXAFS Studies on the Size Dependence of Structural and Dynamic Properties of CdS Nanoparticles. *J. Phys. Chem. B* **1997**, *101*, 2691−2701.
(58) van Bokhoven, J. A.; van der Eerden, A. M. J.; Prins, R. Local Structure of the Zeolitic Catalytically Active Site during Reaction. *J. Am. Chem. Soc.* **2004**, *126*, 4506−4507.
(59) Subila, K. B.; Kishore Kumar, G.; Shivaprasad, S. M.; George Thomas, K. Luminescence Properties of CdSe Quantum Dots: Role of Crystal Structure and Surface Composition. *J. Phys. Chem. Lett.* **2013**, *4*, 2774−2779.
(60) Alexander, S.; Morrow, L.; Lord, A. M.; Dunnill, C. W.; Barron, A. R. pH-responsive octylamine coupling modification of carboxylated aluminium oxide surfaces. *J. Mater. Chem. A* **2015**, *3*, 10052−10059.
(61) Arbi, K.; Hoelzel, M.; Kuhn, A.; Garcia-Alvarado, F.; Sanz, J. Local structure and lithium mobility in intercalated Li3AlxTi2-x(PO4)3 NASICON type materials: a combined neutron diffraction and NMR study. *Phys. Chem. Chem. Phys.* **2014**, *16*, 18397−18405.
(62) Bottke, P.; Rettenwander, D.; Schmidt, W.; Amthauer, G.; Wilkening, M. Ion Dynamics in Solid Electrolytes: NMR Reveals the Elementary Steps of Li+ Hopping in the Garnet Li6.5La3Zr1.75-Mo0.25O12. *Chem. Mater.* **2015**, *27*, 6571−6582.
(63) Gary, D. C.; Flowers, S. E.; Kaminsky, W.; Petrone, A.; Li, X.; Cossairt, B. M. Single-Crystal and Electronic Structure of a 1.3 nm Indium Phosphide Nanocluster. *J. Am. Chem. Soc.* **2016**, *138*, 1510−1513.
(64) Frisch, M. J.; et al. *Gaussian 09*, revision A.1; Gaussian, Inc.: Wallingford, CT, 2009.
(65) Perdew, J. P.; Ernzerhof, M.; Burke, K. Rationale for mixing exact exchange with density functional approximations. *J. Chem. Phys.* **1996**, *105*, 9982−9985.
(66) Adamo, C.; Barone, V. Toward reliable density functional methods without adjustable parameters: The PBE0 model. *J. Chem. Phys.* **1999**, *110*, 6158−6170.
(67) Dolg, M.; Wedig, U.; Stoll, H.; Preuss, H. Energy-adjusted ab initio pseudopotentials for the first row transition elements. *J. Chem. Phys.* **1987**, *86*, 866−872.
(68) Andrae, D.; Häußermann, U.; Dolg, M.; Stoll, H.; Preuß, H. Energy-adjustedab initio pseudopotentials for the second and third row transition elements. *Theor. Chem. Acc.* **1990**, *77*, 123−141.
(69) Martin, J. M. L.; Sundermann, A. Correlation consistent valence basis sets for use with the Stuttgart−Dresden−Bonn relativistic effective core potentials: The atoms Ga−Kr and In−Xe. *J. Chem. Phys.* **2001**, *114*, 3408−3420.
(70) Bergner, A.; Dolg, M.; Küchle, W.; Stoll, H.; Preuß, H. Ab initio energy-adjusted pseudopotentials for elements of groups 13−17. *Mol. Phys.* **1993**, *80*, 1431−1441.
(71) Hehre, W. J.; Ditchfield, R.; Pople, J. A. Self—Consistent Molecular Orbital Methods. XII. Further Extensions of Gaussian—Type Basis Sets for Use in Molecular Orbital Studies of Organic Molecules. *J. Chem. Phys.* **1972**, *56*, 2257−2261.
(72) Francl, M. M.; Pietro, W. J.; Hehre, W. J.; Binkley, J. S.; Gordon, M. S.; DeFrees, D. J.; Pople, J. A. Self-consistent molecular orbital methods. XXIII. A polarization-type basis set for second-row elements. *J. Chem. Phys.* **1982**, *77*, 3654−3665.
(73) Tomasi, J.; Mennucci, B.; Cammi, R. Quantum Mechanical Continuum Solvation Models. *Chem. Rev.* **2005**, *105*, 2999−3094.
(74) Cossi, M.; Barone, V. Time-dependent density functional theory for molecules in liquid solutions. *J. Chem. Phys.* **2001**, *115*, 4708−4717.

DOI: 10.1021/acs.chemmater.8b02468
Chem. Mater. 2018, 30, 5468−5477